Available online at www.sciencedirect.com
SCIENCE DIRECT®
ELSEVIER
Thin Solid Films 455–456 (2004) 619–623
thin solid films
www.elsevier.com/locate/tsf

Generalized ellipsometry for orthorhombic, absorbing materials: dielectric functions, phonon modes and band-to-band transitions of Sb_2S_3

M. Schubert[a,*], T. Hofmann[a], C.M. Herzinger[b], W. Dollase[c]

[a]*Institute for Experimental Physics II, University of Leipzig, Linnéstrasse 5, Leipzig 04103, Germany*
[b]*J.A. Woollam Co., Inc. 645 M Street, Suite 102, Lincoln, NE, 68508, USA*
[c]*Department of Earth and Space Sciences, University of California, Los Angeles, CA 90095, USA*

Abstract

Generalized ellipsometry allows complete extraction of the dielectric function tensor, including orientation, from measurement of skew-cut single crystal orthorhombic absorbing materials. As an example, Stibnite (Sb_2S_3) is studied to determine fundamental phonon modes and band-to-band transitions, which are here provided for polarization along axes *a*, *b*, and *c* from lineshape analysis of the major dielectric function spectra.
© 2003 Elsevier B.V. All rights reserved.

Keywords: Dielectric functions; Band-to-band transitions; Phonon modes; Anisotropy; Generalized ellipsometry; Stibnite

1. Introduction

Complete and accurate sets of optical constants for biaxial (orthorhombic, monoclinic and triclinic) materials, measured over a range of wavelengths, are rare, if they exist at all. Existing methods for determination of optical constants require different, precisely oriented samples. No accurate rigorous method exists so far for monoclinic or triclinic absorbing materials. Measurement of polarization state after Drude [1] (standard ellipsometry) is still valid for appropriately cut and aligned surfaces, but fails for arbitrary orientations (skew cuts) and also when the symmetry is monoclinic or triclinic. Dielectric anisotropy (ignoring magnetic field effects) is analyzed by requiring that the complex dielectric function ε be a symmetric second-rank tensor. For orthorhombic materials, the major values ε_a, ε_b, ε_c for polarization along the crystal axes *a*, *b*, *c*, respectively, and Euler rotation angles φ, ψ, θ fully define the ε tensor within the laboratory frame of Refs. [2,3].

Generalized ellipsometry (GE) is an excellent technique for anisotropic materials characterization, but has been demonstrated mostly for uniaxial situations [2]. This work presents the three fundamental dielectric function spectra of an absorbing orthorhombic material obtained by GE from far-infrared (FIR) to ultra-violet (UV) wavelengths, using several, differently cut surfaces from mechanically polished single crystals. Stibnite is used exemplarily. This current study revisits work on stibnite (Sb_2S_3) reported many years ago by Drude (1888) [4] and Tyndall (1927) [5], who measured ε_b and ε_c for this material at a few select wavelengths on natural cleavage surfaces. The present report fills in lacking data along axis *a*, and extends spectral coverage. FIR-active phonon modes, critical-point (CP) parameters of electronic band-to-band transitions and dielectric functions along axes *a*, *b* and *c*, most of which were previously unpublished, are provided. GE is demonstrated to overcome constraints and limitations of Drude's standard ellipsometry.

Scattered reports exist on optical properties of stibnite (P*nma*, $a=11.310$ Å, $b=3.8389$ Å, $c=11.299$ Å, cleavage is (100) perpendicular to *a* [6]) [7,8]. Band-gap measurements [7,9], band structure calculations [9] and phonon modes for polarization along axes *b* and *c* were reported [10]. Data from reflectivity measurements (0.7eV to 12.5eV) and tentative reflectivity peak assignments for band-to-band transitions are available [11].

1.1. Generalized ellipsometry

Generalized ellipsometry, introduced originally by Azzam and Bashara [12], determines three ratios of reflection coefficients for polarized light out of the four

*Corresponding author. Fax: +49-3419736249.
E-mail address: mschub@physik.uni-leipzig.de (M. Schubert).

0040-6090/04/$ - see front matter © 2003 Elsevier B.V. All rights reserved.
doi:10.1016/j.tsf.2003.11.207

complex-valued elements of the Jones reflection matrix **r**. Off-diagonal elements in **r** are non-zero for surfaces, which convert incident p into reflected s waves, and vice versa. The GE parameters Ψ_{ij}, Δ_{ij} are defined by [2]

$$\frac{\mathbf{r}_{pp}}{\mathbf{r}_{ss}}=\tan\Psi_{pp}\exp(i\Delta_{pp}),$$

$$\frac{\mathbf{r}_{ps}}{\mathbf{r}_{pp}}=\tan\Psi_{ps}\exp(i\Delta_{ps}),$$

$$\frac{\mathbf{r}_{sp}}{\mathbf{r}_{ss}}=\tan\Psi_{sp}\exp(i\Delta_{sp}), \tag{1}$$

$$\mathbf{r}=\mathbf{r}_{ss}\begin{pmatrix}\mathbf{r}_{pp}/\mathbf{r}_{ss} & \mathbf{r}_{sp}/\mathbf{r}_{ss}\\ \mathbf{r}_{ps}/\mathbf{r}_{ss} & 1\end{pmatrix}=\mathbf{r}_{ss}\begin{pmatrix}\rho_{pp} & \rho_{sp}\\ \rho_{ps}\rho_{pp} & 1\end{pmatrix} \tag{2}$$

Ψ_{ij} and Δ_{ij} depend on the tensor ε, the ambient medium's index of refraction, and the angle of incidence Φ_a. The elements of ε follow by comparing calculated data to measured data as part of a standard least-square fit procedures. In addition to Ψ_{ij}, Δ_{ij}, the standard deviations $\sigma^{\Psi ij}$ and $\sigma^{\Delta ij}$ are estimated as part of the measurement procedure, and propagated into the error bars on the resulting fit parameters [13].

2. Experimental

Samples studied here were cut approximately parallel to (100) ('*a*-plane'), (010) ('*b*-plane'), (001) ('*c*-plane'), and (313) from a single crystal (details are in Ref. [8]). GE data were measured as explained in Ref. [8], specifically at $\Phi_a=20$–$70°$ (NIR-UV) and 40–70° (FIR), at φ =0–360° (sample azimuth), for wave numbers $\omega=75$–350 cm^{-1} (FIR) in steps of 1 cm^{-1}, and for $\lambda=300$–1700 nm (NIR-UV) in steps of 10 nm. An in-house built Fourier-transform-based generalized Mueller FIR ellipsometer [14] and a commercial NIR-UV ellipsometer (J.A. Woollam Co.) were employed.

3. Results and discussion

Fig. 1 presents selected FIR-GE data for *a*-, *b*- and *c*-plane samples. Calculated data were obtained by the wavelength-by-wavelength data inversion approach fitting for ε_a, ε_b, ε_c and all respective Euler angles upon inclusion of all measurements (multiple-sample-, -angle-of-incidence-, -sample-azimuth-analysis). Precise sample orientation and crystal cuts are not required as these are included in the Euler angles and are determined as part of the data fitting process. Data in (a) and (b) were taken with the *c*-axis oriented nearly parallel and perpendicular to the plane of incidence, respectively. Data

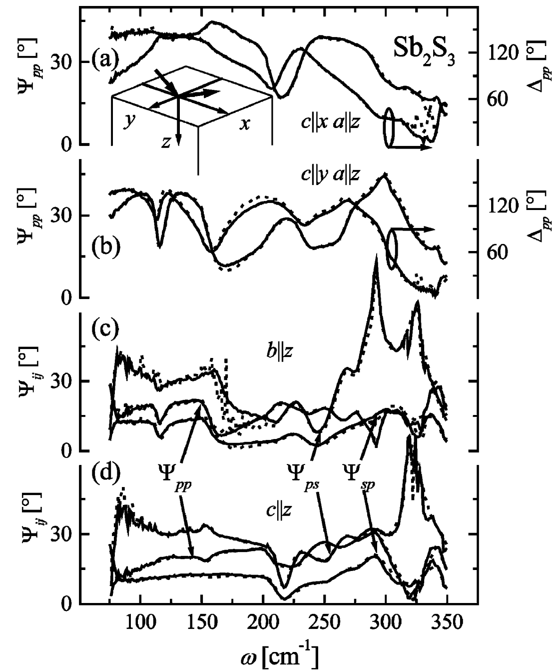

Fig. 1. Experimental (dotted lines) and best-fit calculated FIR-GE data (solid lines), exemplified by nearly *a*-plane (a), (b), *b*-plane (c), and *c*-plane (d) oriented Sb_2S_3 surfaces. For (c) and (d), the angle between the stibnite *a*-axis and the laboratory coordinate *x* is approximately 45°. Ellipsometer plane of incidence is (*x*,*z*), the sample surface is (*x*,*y*).

in (c) and (d) (Δ_{ij}-spectra omitted for brevity) were acquired with the *a*-axis oriented approximately halfway between the laboratory *x*- and *y*- axes, i.e. ~45° rotated off the plane of incidence. Fig. 2 summarizes functions ε_a, ε_b, and ε_c. Dotted lines are the wavelength-by-wavelength fit results. Solid lines are best-fit data using anharmonic Lorentzian-broadened oscillator model functions [14]. Phonon mode resonance and broadening parameters resulting from the lineshape model are summarized in Table 1, in comparison with results from Riede [10]. The agreement between phonon modes from FIR-GE and polarized FIR reflectivity is very good. No comparison data are available for the *a* polarization, which is not contained within natural cleavage faces. The generalized Lowndes condition for the damping parameters is satisfied for all phonon mode branches [14]. The high-frequency dielectric constants parameters were estimated from the NIR-UV data as $\varepsilon_{\infty,c}=10.8$, $\varepsilon_{\infty,b}=12.5$ and $\varepsilon_{\infty,a}=7$.

Fig. 3 depicts selected experimental and calculated NIR-UV Ψ_{pp} data, exemplified by (313)-plane Sb_2S_3, at 60° separated sample azimuths. The Euler angles for axes *a*, *b*, *c* are φ =54.5°+*m*60° (*m*=1–5), ψ=−38.5° and θ= 54.6°. All other spectra are omitted for brevity. Calculated data were obtained by the same wavelength-by-wavelength analysis procedure. Surface orientations obtained from the NIR-UV and FIR best-fit

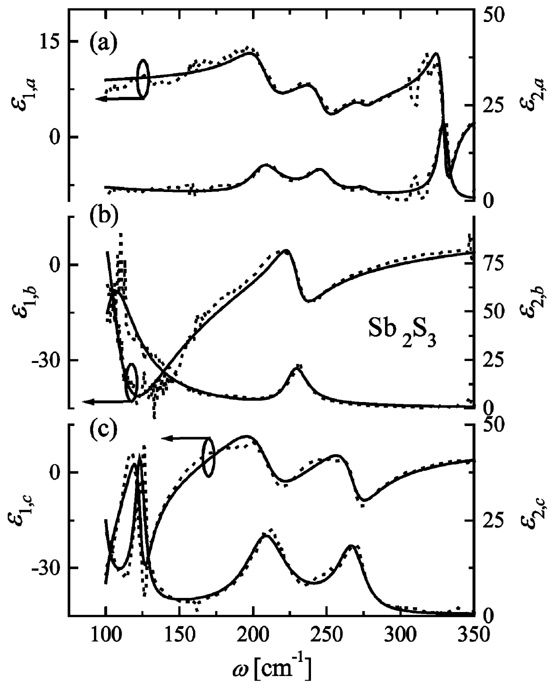

Fig. 2. Real (ε_1) and imaginary part (ε_2) of the FIR dielectric functions of stibnite for polarizations along crystallographic axes *a* (a), *b* (b), and *c* (c). Dotted lines: wavelength-by-wavelength data inversion; Solid lines: Anharmonic Lorentzian-broadened oscillator model.

regressions are highly consistent with the results in Ref. [8] obtained at $\lambda = 589$ nm. This is expected for orthorhombic symmetry, which does not exhibit dispersion of optical axis orientation. Spectra for ε_a, ε_b, ε_c, obtained from the wavelength-by-wavelength analysis and from subsequent lineshape analysis using Lorentzian-broadened harmonic oscillators are depicted in Fig. 4. Band-to-band transitions produce CP structures within the dielectric functions due to singularities within the joint-density-of-states function. To first-order approximation and within sufficient accuracy in the present case, harmonic oscillator ensembles enable adequate model description of the CP structures observed in Fig. 4. Table 2 summarizes the oscillator center frequencies (vertical arrows in Fig. 4). Fig. 5 shows a NIR-UV three-dimensional surface plot of ρ_{ps} data (imaginary

Table 1
Room temperature transverse and longitudinal optical phonon mode frequencies of Sb_2S_3 in units of cm^{-1} for polarization along crystal axis *a*, *b*, and *c*, determined from FIR dielectric function lineshape analysis. Values in parentheses represent the 90% confidence interval for the last digit

j	Riede[a] (FIR-reflectivity)		Present work (FIR-ellipsometry)			
	ω_{TO}	ω_{LO}	ω_{TO}	ω_{LO}	γ_{TO}	γ_{LO}
E‖*a*						
1	–	–	206(1)	215(2)	26(2)	33(4)
2	–	–	247(2)	255(2)	20(3)	12(3)
3	–	–	273(2)	276(2)	12(5)	12(5)
4	–	–	329(1)	343(1)	8(1)	6(1)
E‖*b*						
1	120.0	203.3	101.5(5)	211(1)	30(1)	17(3)
2	230.0	290.0	229(1)	300(3)	18(2)	29(8)
E‖*c*						
1	94.8	112.5	98(1)	113.5(5)	25(2)	7(2)
2	123.0	153.5	122.8(4)	157(1)	9(1)	19(5)
3	208.0	232.0	209(1)	238(2)	33(2)	40(4)
4	264.0	306.5	268(1)	307(2)	21(2)	18(4)

[a]V. Riede, Ann. Phys. 25, 415 (1970). No confidence intervals were given.

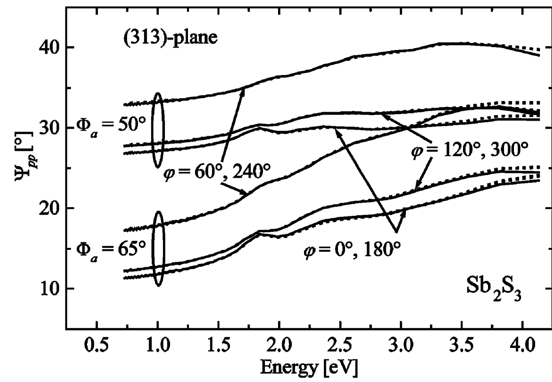

Fig. 3. Experimental (dotted lines) and best-fit (solid lines) calculated NIR-UV Ψ_{pp} data are shown for an approximately (313)-plane oriented Sb_2S_3 surface at various sample azimuths φ.

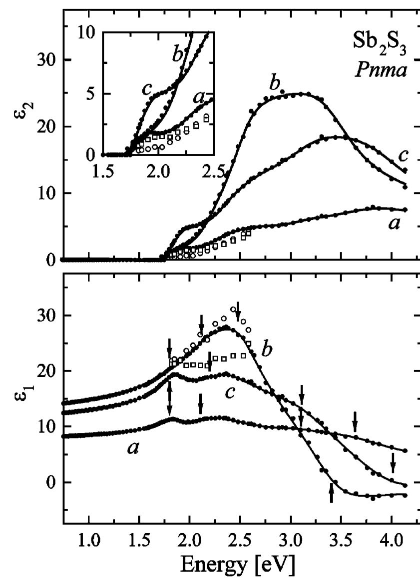

Fig. 4. NIR to UV dielectric functions of stibnite for polarizations along crystallographic axes *a*, *b* and *c*. Solid symbols: wavelength-by-wavelength inverted data. Solid lines: best-fit harmonic oscillator lineshape functions with center frequencies indicated by vertical arrows. Open symbols are data reproduced from Drude and Tyndall (□: ε_c, ○: ε_b).

Table 2
Sb_2S_3 CP transition energies in units of eV for polarization along crystal axis *a*, *b* and *c*, determined from NIR-UV dielectric function lineshape analysis. Values in parentheses represent the 90% confidence interval for the last digit

CP	Shutov et al.[a] (Polarized reflectivity)		Present work (NIR-UV-ellipsometry)		
	$E\|a$ and $E\|c$	$E\|b$	$E\|a$	$E\|b$	$E\|c$
E_1	1.88		1.82(2)	1.80(4)	1.80(4)
E_2	2.56		2.09(3)	2.10(5)	2.20(3)
E_3		2.68	3.08(2)	2.48(3)	3.09(2)
E_4		3.32		3.40(4)	
E_5	3.48–3.8 4.6	3.55–3.82 4.54	3.61(6)		4.02(1)

[a]Shutov et al., Phys. Stat. Sol. 31, K23 (1969). Energies follow from intensity peak assignment.

part only) for an approximate (313)-plane of stibnite vs. relative sample azimuth φ_0. Data in Fig. 5 were calculated using the wavelength-by-wavelength best-fit dielectric functions shown in Fig. 4. In Fig. 5 it was assumed $\theta=\psi=\varphi=45°$. The in-plane azimuth φ_0 then relates the sample in-plane azimuth with the plane of incidence. At $\varphi_0=0$, inverse rotation by $\theta=\psi=\varphi=-45°$ would align the stibnite major axes *a*, *b*, *c* with the Ellipsometer (i.e. laboratory) axes *x*, *y*, *z*, respectively. Note that *x* is parallel to the plane of incidence and the sample surface, the origin of (x,y,z) is set at the surface, and *z* points towards the interior of the sample. For definition and instructions one may refer to Ref. [3]. This surface plot sheds light on the sample anisotropy, but is most intriguing because one can recognize the CP structures adherent to the individual dielectric functions. This plot provides visual evidence that the dielectric functions for orthorhombic bulk materials can be

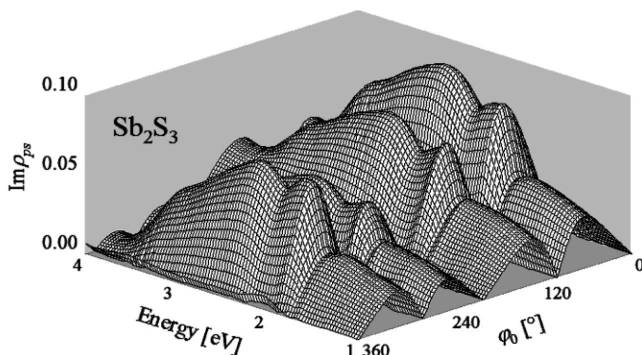

Fig. 5. NIR-UV imaginary part of $\rho_{ps}=\mathbf{r}_{ps}/\mathbf{r}_{pp}$ for an approximate (313)-plane of stibnite vs. relative sample azimuth φ_0 ($\Phi_a=65°$). The three-dimensional plot contains calculated data using the dielectric functions shown in Fig. 4.

obtained by studying the optical response from a single skew-cut surface.

Data reported by Shutov et al. [11] are included in Table 2 as well, with fair agreement with our data, likely because no lineshape analysis was performed in Ref. [11]. Shutov et al. noted essentially no difference between spectra taken with polarization along *a* and *c*, and assigned this observation to polishing effects, reflecting the aforementioned inevitable incertitude of the reflection intensity approach. Open symbols in Fig. 4 depict data reproduced from Drude [4] and Tyndall [5]. Discrepancies occur likely because of surface overlayer effects. Tyndall and Drude noted change of reflectivity of freshly cleaved stibnite over time. As will be reported in detail elsewhere, surface overlayer effects must be accounted for by considering the time-dependence of the measurement course using a simple overlayer growth model.

4. Conclusions

Fundamental phonon modes and band-to-band transitions are provided for polarization along axes *a*, *b*, and *c* from lineshape analysis of the major dielectric function spectra for orthorhombic Sb_2S_3.

Generalized ellipsometry is uniquely suitable for the precise determination of anisotropic optical functions spectra of biaxial materials, most of which are largely unstudied at this time. We expect GE to be fully applicable to triclinic and monoclinic materials.

Acknowledgments

The authors acknowledge Prof. John A. Woollam of the University of Nebraska-Lincoln (UNL) for continuing interest. Financial support for this study was provided in part by UNL.

References

[1] P. Drude, Annalen der Physik. 32 (1887) 584.
[2] M. Schubert, Generalized ellipsometry, in: W.S. Weiglhofer, A. Lakhtakia (Eds.), Introduction to Complex Mediums for Optics and Electromagnetics, SPIE, Bellingham, WA, 2003.
[3] M. Schubert, Theory and application of generalized ellipsometry, in: G.E. Irene, H.W. Tompkins (Eds.), Handbook of Ellipsometry, Noyes Publications, 2004.
[4] P. Drude, Annalen der Physik Leipzig 34 (1888) 489.
[5] E.P.T. Tyndall, Phys. Rev. 21 (1923) 162.
[6] Semiconductors other than group IV and III–V compounds, in: R. Poerschke, O. Madelung, (Eds.), Data Science and Technology, Springer, Berlin, 1992. This source uses the (historical) *Pbnm* assignment instead of *Pnma*.
[7] A.G. Vesdeshwar, J. Phys. III Fr. 5 (1995) 1161.
[8] M. Schubert, W. Dollase, Opt. Lett. 27 (2002) 2073.

[9] T. Fujita, K. Kurita, K. Takiyama, T. Oda, J. Phys. Soc. Jpn. 56 (1987) 3734.
[10] V. Riede, Annalen der Physik Leipzig 25 (1970) 415, 7th Series.
[11] S.D. Shutov, V.V. Sobolev, Y.V. Popov, S.N. Shestatskii, Phys. Status Solidi 31 (1969) K23.
[12] R.M.A. Azzam, N.M. Bashara, J. Opt. Soc. Am. 62 (1972) L1521.
[13] G.E. Jellison Jr, Data analysis for spectroscopic ellipsometry, in: G.E. Irene, H.W. Tompkins (Eds.), Handbook of Ellipsometry, Noyes Publications, 2004.
[14] M. Schubert, Infrared ellipsometry on semiconductor layer structures: phonons, plasmons and polaritons, Series Springer Tracts in Modern Physics, Springer, Heidelberg, 2004, in preparation.